STUDY OF Zn-Ni ALLOY COATINGSMODIFIED BY NANO-AL_2O_3 PARTICLES INCORPORATION

Malika Diafi [1)], Said Benramache [1)] Elhachmi Guettaf Temam [1)], Adaika Mohamed Lakhdar [1)], Brahim Gasmi [1)]*

[1)] *Physic Laboratory of Thin Films and Applications (LPCMA), University of Biskra, 07000, Algeria*

Received: 27.03.2016
Accepted: 11.07.2016

[*]Corresponding author: *e-mail: diafimalika@gmail.com, Tel.: +213557286468, Physic Laboratory of Thin Films and Applications (LPCMA), University of Biskra, 07000, Algeria*

Abstract

$Zn–Ni–Al_2O_3$ nano-composite coatings were electrodeposited on mild steel using a novel sol enhanced electroplating method. The effect of alumina sol on the electrodeposition process, and coating properties was investigated using, X-ray diffraction, scanning electron microscopy (SEM), measurement of microhardness and chronoamperometry and electrochemical impedance spectroscopy were studied in a solution of 3% NaCl. The results indicated that the electro-crystallization processes of Zn–Ni and $Zn–Ni–Al_2O_3$ were governed by a three-dimensional nucleation process controlled by diffusion. XRD results showed that the phase structure of both alloy and composite coatings was single Ni_5Zn_{21}-γ phase, and the addition of alumina sol in the Zn-Ni matrix increases the microhardness, and we note the maximum hardness is obtained for 50 g/L Al_2O_3. Conversely, these coatings showed smaller crystallite size and Surface of coatings was uniform and compact, the values of R_{ct} and Z_w increase, while the values of C_{dl} decrease with increasing alumina nano-particles content values for the Zn–Ni– Al_2O_3 alloy clearly confirm the better corrosion resistance.

Keywords: Al_2O_3, Nickel, Zinc, EIS, XRD, SEM, chronopotentiometry

1 Introduction

Electroplated binary Zn–Malloys, where metals are an Fe group such as Ni, Co and Fe, exhibit improved properties compared to pure Zn [1-5]. It is well-known that zinc alloys can provide protection of steel against corrosion, with Zn–Ni, Zn–Co and Zn–Fe being most commonly used [6, 7]. The use of specific bath additives has also been found beneficial with respect to corrosion resistance, even for low contents of Metals [6]. Electrodeposited Zn–Ni alloys exist in the form of three dominant phases: α, γ and η. The α-phase is a solid solution of Zn in Ni with an equilibrium solubility of about 30 % Zn. The η-phase is a solid solution of Ni in Zn, with a Ni solubility of less than 1 %. The composition range of the pure γ-single phase was determined to be between 10 and 30 % Ni. The amount of Ni in the alloy, which finds industrial application in the corrosion protection field, is around 15% and its dominant structure is the γ-phase $Zn_{21}Ni_5$ [8], Electroplated co-deposition is widely used for preparing metal matrix composite coatings because of its low cost and versatility. Electroplated co-deposition is widely used for preparing metal matrix composite coatings because of its low cost and versatility. In general, hard oxide (Al_2O_3, TiO_2, and SiO_2) or carbide particles (SiC and WC), or even diamond and carbon nanotubes (CNT) are

DOI 10.12776/ams.v22i3.706 p-ISSN 1335-1532
e-ISSN 1338-1156

used as a second phase [9] and established applications and possess good chemical stability, high microhardness, and good wear resistance and corrosion resistance at elevated temperature [9–14]. Zn–Ni composite coatings for example Zn–Ni–Al_2O_3 [9, 10, 15, 16], Zn–Ni–TiO_2 [11, 17], Zn–Ni–SiO_2 [13] and Ni–Zn–P [14], ZnNi–SiC [16, 18], this research work was to codeposit nano-Al_2O_3 particles into the Zn-Ni alloy coatings deposits on a mild steel substrate. In order to improve the surface properties and the corrosion resistance in aggressive media. Then, the composite coatings had been characterized, morphological (SEM), structural (XRD), and electrochemical properties of the composite coatings had been studied by potentiodynamic polarization and electrochemical impedance spectroscopy in a solution of 3 % NaCl.

2 Experimental

2.1 Coating processes

The deposition of Zn–Ni coatings was carried out onto steel substrates under galvanostatic conditions at operating current density of 30 A cm^{-2} and a temperature of 30°C, the chemical composition of the basic electrolyte of Zn–Ni alloys deposition was given in **Table 1** [8]. Electrodeposits Zn–Ni were obtained by varying the concentration of Al2O3 in the bath (0, 30, 50 $g \cdot L^{-1}$).

2.2 Coating characterization

XRD characterization of samples was carried out with a D8 Advance-Brucker using a Cu Kα line at λ= 0.1540 nm in the 2Θ ranged of 10–95° in steps of 0.02° at a scan speed 2°/min. Bruker GAADS soft-ware was utilized to calculate.

Table 1 Electrolyte I composition and conditions for alloy plating.

Electrolyte I ingredients	**Concentration ($g \cdot L^{-1}$)**	**Plating parameters**
$ZnSO_4 \cdot 7H2O$	57.5	30 °C and pH=3-4,5 constant current densities at 10 mA cm^{-2} for 60 s
H_3BO_3	9.3	
Na_2SO_4	56.8	
$Na_3C_6H_5O_7$	56.8	

The biaxial stress along the lateral and longitudinal directions with 2D area detector using a standard 2Θ sin2Ψ method [19]. The average grain size of the coatings was determined from X-ray peak broadening by applying the Scherrer formula [20, 21]:

$$D = \frac{0.9\lambda}{\beta cos\theta} \quad (1.)$$

where D is the grain size, is the X-ray wavelength (λ = 1.5406 A), β is the full width at half-maximum (FWHM), and θ is Bragg angle position of peak. For (330) reflections and peak broadening was measured by the integral width method [22], Surface morphology of the deposits was followed with A JEOL (model JSM6390LV), Microhardness of coatings was measured using a load of 100 g with a holding time of 15 s by using a Vickers hardness tester (HV) of deposits were performed in the surface by using a Wolpert Wilson Instruments (model 402UD) [23].
Corrosion behavior and protection performance of Zn–Ni and Zn–Ni–Al_2O_3 alloy coatings was studied by using electrochemical impedance spectroscopy (EIS) and electrochemical Tafel

DOI 10.12776/ams.v22i3.706 p-ISSN 1335-1532
e-ISSN 1338-1156

extrapolation in 3 % NaCl solution. The tests were performed using a potentiostat /galvanostat (using a Volta Lab 40), the working electrode was a coated sample, the counter electrode was platinum with an area of 1 cm^2 and the reference electrode was Hg/HgO/ 1 M KOH. All potentials in the text have been referred to this reference electrode. Electrochemical impedance spectroscopy (EIS) measurements were obtained at the open circuit potential (OCP) in a frequency range of 10 kHz–0.001 Hz, with an applied AC signal amplitude perturbation of 10 mV. During the measuring process of Tafel polarizing curves, the polarization curve scanning rate was 5 mV/s, with a scanning range from –0.25 V of open circuit potential to +0.25 V of open circuit potential. The E_{Corr} and I_{Corr} were determined from the intercepts by Tafel extrapolation method .The chronoamperometric studies were conducted to identify the nucleation mode of Zn–Ni–Al_2O_3 composite and Zn–Ni alloy coatings at potentials E=500mv, vs. Hg/HgO applied for 1 hours of 3% NaCl. This potentiostatic technique has proved to be a powerful tool for evaluation of the nucleation mode by electrocrystallization

3 Results and discussions

3.1 X-ray diffraction

Fig.1 shows the XRD results for Zn–Ni composite coatings, the phase structure is single γ-Ni_5Zn_{21} phase [2, 10]. The grain sizes, being the (330) plane always the most intense, crystallite sizes of the coatings were calculated from the X-ray peak broadening of the (330) diffraction peak using Scherrer's formula , which is well suited to detect grain diameters less than 100 nm, and has been used widely for Zn–Ni deposits [10, 24]. The grain sizes of all of the coatings were on a nanometer scale, confirming the nanocrystalline structure of coatings. Zn–Ni–Al_2O_3 coatings showed a smaller grain size compared to the Zn–Ni alloy coating. Zn–Ni alloy deposited in electrolyte I, exhibited a crystallite size of 45 nm, whereas the crystallite size of Zn–Ni alloy coating deposited in electrolyte I+50 $g \cdot L^{-1}$ Al_2O_3 decreased to 24 nm. This finer structure presence of smaller grains explained probably the increase microhardness.

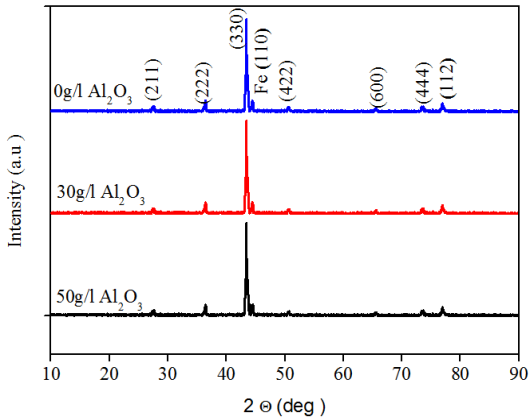

Fig. 1 XRD patterns of Zn–Ni alloy coatings electrodeposited onto steel substrate at different concentrations of Al_2O_3). Composite coatings were deposited at 30 mA/cm^2, T = 30 °C, and pH 3-4, 5 for 60 s.

3.2 Surface morphology

The morphology of these coatings plated in different compositions is presented in **Fig. 2**, further that the Zn–Ni alloy exhibits a uniform [8], Zn-Ni-Al_2O_3 composite coating was uniform and

DOI 10.12776/ams.v22i3.706 p-ISSN 1335-1532
e-ISSN 1338-1156

compact, with a fine grained morphology. Therefore, the presence of Al_2O_3 in the electroplating bath and incorporation of Al_2O_3 in the Zn–Ni coating, increased refinement of crystal size [10],

3.3 Effect of Al_2O_3 content in the bath on microhardness of the coatings

The microhardness of Zn–Ni alloy and the Zn–Ni–Al_2O_3 nanocomposite coatings results are presented in **Fig. 3**, the microhardness of the nanocomposite coatings increases with increasing weight percentage of the nano- Al_2O_3. The hardness increased from 246 Hv for Zn–Ni [8], alloy to 350 and 383 Hv for 30 and 50 g /l Al_2O_3 nanocomposite coating respectively. Microhardness of composite coatings containing Al_2O_3 has been attributed to the hindraness of dislocation movement by Al_2O_3 particles [9, 15, 25], the microhardness of nanocomposite coating depends directly on the alumina content of nanocomposite coating.

Table 2 Values of micro-hardness Vickers hardness (HV) registered different electro deposition

Coating	hardness **(HV)**
Steel	167.7
Zn Ni	246
Zn-Ni-Al_2O_3 (30 g /l)	350
Zn-Ni-Al_2O_3 (50 g /l)	383

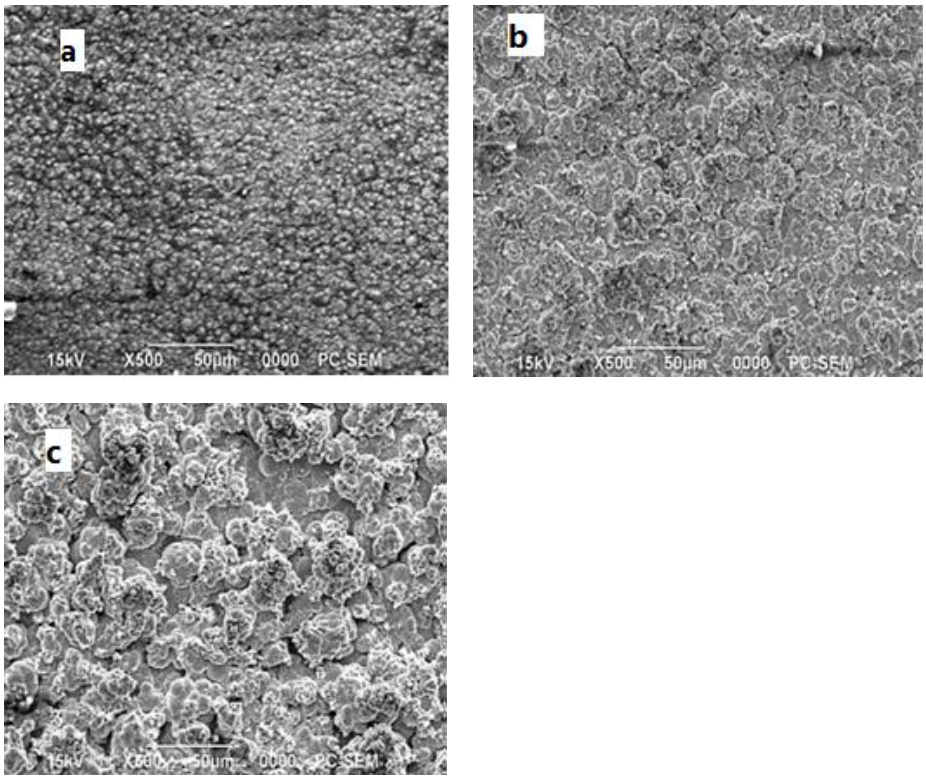

Fig. 2 Surface morphology of (a) Zn–Ni alloy coatings and (b) Zn–Ni–Al_2O_3 (30 g /l Al_2O_3), (c) Zn–Ni–Al_2O_3 (50 g /l Al_2O_3) Composite coatings deposited at 30 mA/cm2, T = 30 °C, and pH 3-4,5 for 60 s.

DOI 10.12776/ams.v22i3.706 p-ISSN 1335-1532
e-ISSN 1338-1156

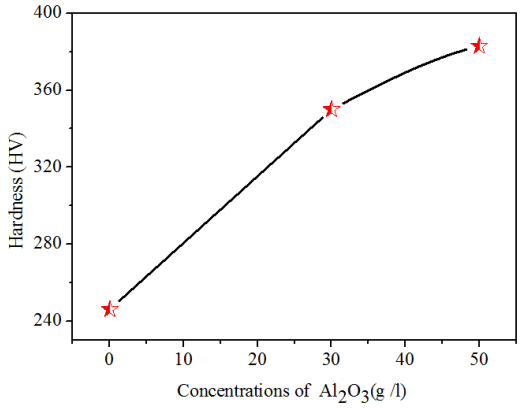

Fig. 3 The effect of nano-alumina contents in the composite coatings on the hardness of deposits. Zn–Ni alloy and Zn–Ni–Al_2O_3 nanocomposite coatings

3.4 Corrosion studies

3.4.1. Potentiodynamic polarization studies

Fig. 4 shows the Tafel curves measured for the Zn–Ni alloy coating and Zn–Ni–Al_2O_3 nanocomposite coating in 3 % NaCl solution ,The corrosion potentials and corrosion currents calculated from Tafel plots [12] , The corrosion potential E_{corr} ,the polarization resistance R_p and corrosion current (i_{corr}). Values were determined from this figure and cited in **Table 3**. The corrosion potential and corrosion current for the Zn-Ni-Al_2O_3 (50 g /l) nanocomposite coating, obtained from the polarization curves were -1,0376 V and 0.255 mA/cm^2 respectively and those for the Zn–Ni alloy coating were determined to be -1,0614 V and 0.1025 mA/cm^2 respectively. It is seen that the nanocomposite coatings higher positive corrosion potentials and smaller corrosion current densities than that of Zn–Ni alloy coating. The Zn–Ni–Al_2O_3 nanocomposite coatings have better corrosion resistance than that of Zn–Ni alloy, the corrosion potential increased with the increase of nano-alumina content [15].

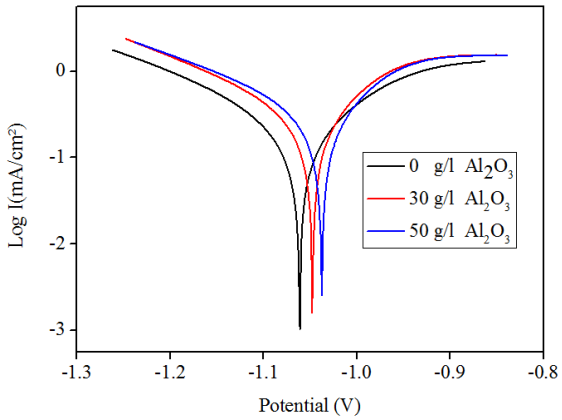

Fig. 4 Polarizing curves obtained for the alloy coatings in a 3 % NaCl solution at different concentrations of Al_2O_3

DOI 10.12776/ams.v22i3.706 p-ISSN 1335-1532
e-ISSN 1338-1156

Table 3 The electrochemical parameters (E_{corr}, I_{Corr}, β_a, β_c) of the coatings samples in a 3 % NaCl solution

Coating	E_{corr} (mV)	I_{corr} (mA/cm^2)	β_a (mV/dec)	β_c (mV/dec)	Rp (Ω cm^2)
Zn Ni	-1061	0.255	246,2	-259,4	169.13
Zn-Ni-Al_2O_3 (30 g /l)	-1047	0.159	180,9	-256,8	103.19
Zn-Ni-Al_2O_3 (50 g /l)	-1037	0.102	157,5	-215,0	109.43

3.4.2. Electrochemical impedance spectroscopy (EIS) studies

Fig. 5 presents a comparison of Nyquist responses obtained for Zn-Ni alloy coatings and Zn-Ni alloy composites elaborated under the same quantities of electricity in 3% NaCl solution. L'impédance, Dans le Plan de Nyquist, is represented by a boucle capacitive.

The data of the charge transfer resistance, Rct and the capacity of the double layer (Cdl) were calculated using both the Nequist and Bode plots of the impedance spectrum (**Table 3**). However, the Warburg impedance (Zw) is determined from the following equations:

$$Z' = \sigma \frac{1}{\omega^{1/2}} - j \frac{\sigma}{\omega^{1/2}} \quad (2.)$$

$$|Z'| = \frac{\sqrt{2}\sigma}{\omega^{1/2}} \quad (3.)$$

The Warburg coefficient σ, can be determined from the slope of the Warburg plot (the slope of real parts of Z' vs. $1/\omega^{1/2}$; $\omega=2\pi F$), or by fitting to an equivalent circuit model which includes a Warburg impedance. However, most equivalent circuit modeling programs return "Z_w" rather than σ, Z_w is the Warburg impedance (Zw =W) which are calculating from the following equation (**Table 4**):

$$\sigma = \frac{1}{Z_{\omega\sqrt{2}}} \quad (4.)$$

The data of the charge transfer resistance, R_{ct}, and the capacity of the double layer (C_{dl}) were calculated using both the Niequist and Bode plots of the impedance spectrum (**Table 4**) is determined from the following equations:

The R_{ct} can be related to i_{Corr} [26]

$$R_{ct} = \frac{b_a\, b_c}{2.3(b_a b_c) i_{corr}} \quad (5.)$$

R_{sol}: solution resistance
R_{ct}: charge transfer resistance
b_a and b_c anodic and cathodic tafel slopes

The double layer capacitance C_{dl} can be related to Z_{ima} max [26]

$$\omega(Z_{ima}\max) = \frac{1}{R_{dl}C_{dl}} \quad (6.)$$

From the data obtained in **Table 3**, one can conclude that the values of Rct and Zw increase, while the values of Cdl decrease with increasing alumina nano-particles content, and this behavior is in good agreement with that obtained of the Tafel plot measurements ,the spectra presented show at least two time constants. The first time constant, recorded at higher frequency,

DOI 10.12776/ams.v22i3.706 p-ISSN 1335-1532
e-ISSN 1338-1156

is displayed as a depressed incomplete semicircle. The electrical-equivalent-circuit (EEC) parameters, describing the process included in this time constant are Rct and C_{dl} [27, 28]. The second time constant, depicted at lower frequencies, corresponds to a straight line Figs 6 .This linear dependence between the imaginary and real part of the capacitance is related to the diffusion process of the soluble species, while is called Warburg impedance (Z_w). Therefore, EEC parameters describing the process included in the second time constant clearly indicates the diffusion control of the soluble species. From the electrode surface to the bulk of solution [27, 28]. Zn–Ni– Al_2O_3 provides better protection against corrosion on the steel substrate [13].

Table 4 Extracted fitted data from the equivalent circuit of Zn–Ni alloy coatings in a 3 % NaCl

Coating	R_p ($\Omega.cm^2$)	R_s ($\Omega.cm^2$)	R_{ct} ($\Omega \cdot cm^2$)	C_{dl} ($\mu F/cm^2$)	(Zw) ($\Omega \cdot cm^2$)
Zn Ni	1.259	0.405	78.5	1.310	0.669
Zn-Ni-Al_2O_3(30g /l)	1.762	0.677	135	0.936	0.8 27
Zn-Ni-Al_2O_3 (50 g /l)	1.797	0.697	183	0.918	1.157

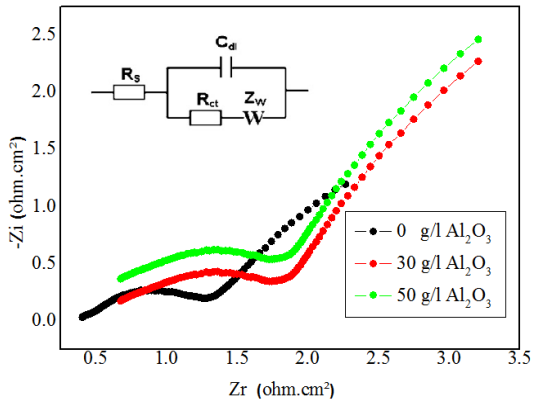

Fig. 5 The Nyquist plots obtained Zn–Ni–Al_2O_3 composite and Zn–Ni alloy coatings electrodeposited at different concentrations of Al_2O_3

3.4.3. Chronoamperometry studies

The chronoamperometric studies were conducted to identify the nucleation mode of Zn–Ni–Al_2O_3 composite and Zn–Ni alloy coatings at potentials E=500mv. The chronoamperometric studies were performed at 30 °C vs. Hg/HgO applied for 1 hour of 3 % NaCl. **Fig. 7**, the transients can be divided into two regions. The first region corresponds to the increase in current density up to a maximum, which is typical of crystal nucleation and growth processes. During this stage, the nuclei develop diffusion zones around themselves. The second region corresponds to the decrease in the current density, which is typical of a diffusion-controlled process [10, 29-31]. Scharifker and coworkers derived analytical expressions for multiple nucleation phenomena followed by diffusion-controlled growth of three-dimensional islands. The resulting expressions for the normalized current densities allow to distinguish between instantaneous nucleation and progressive nucleation, according to Eq. (5) for instantaneous nucleation and Eq. (6) for progressive nucleation:

DOI 10.12776/ams.v22i3.706 p-ISSN 1335-1532
e-ISSN 1338-1156

$$\left(\frac{I}{I_m}\right)^2 = 1{,}9542\,\frac{t_m}{t}\left[1-\exp(-1{,}2564\,\frac{t}{t_m})\right]^2 \quad (7.)$$

$$\left(\frac{I}{I_m}\right)^2 = 1{,}2254\,\frac{t_m}{t}\left[1-\exp\left(-2{,}3367\,\frac{t}{t_m}\right)\right]^2 \quad (8.)$$

The experimental and theoretical data for Zn–Ni alloy and Zn–Ni–Al_2O_3 deposition a potentials E=500mv are shown in **Fig. 8a** and **8b**. In these figures, the instantaneous nucleation rate is higher than the progressive nucleation rate [10, 25, 26]. As seen in **Fig. 5**, the experimental data more closely approximated theoretical progressive curve for the Zn–Ni alloy coating (**Fig. 8a**). Thus, the progressive nucleation mode would be predominant for the Zn–Ni alloy. However, for the Zn–Ni composite coating, the nucleation mode was closer to instantaneous nucleation (**Fig. 8b**). This difference may be explained by the adsorption of alumina nano-particles on the cathode surface which created additional active nucleation sites during electrodeposition on the mild steel substrate [10].

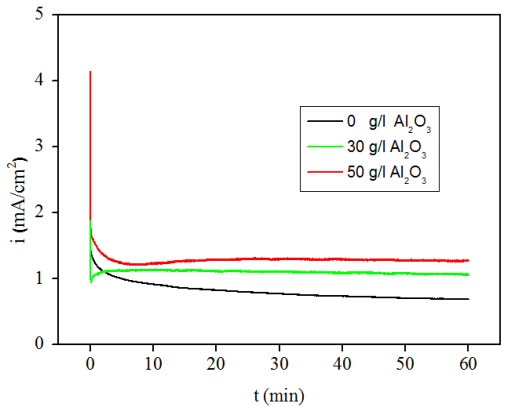

Fig. 6 Chronoamperograms of Zn–Ni–Al_2O_3 composite and Zn–Ni alloy coatings at potentials E=500mv, vs. Hg/HgO applied for 1 hour of 3 % NaCl

4 Conclusion

This work represented the electrodeposition and the corrosion behavior of Zn-Ni alloy deposits elaborated in absence or in presence of 30 and 50 g /l of nano-Al_2O_3 in the acid sulfate bath. This study was made to evaluate the influence of nanoparticles addition on some properties such as hardness, morphologic structure characteristics, and corrosion resistance the results revealed that of Zn–Ni alloy and the Zn–Ni–Al2O3 nanocomposite coatings:

- XRD and SEM results indicate all the Zn-Ni alloy coatings have similar phase composition (γ-phase structure), with smaller crystallite size
- The deposited coating with 50g/l Al2O3 showed the maximum value of hardness 383HV, because the increase of nano-Al_2O_3 concentration in the plating bath increases of micro-hardness.
- The corrosion potential increased with the increase of nano-alumina content, while the corrosion current decreased from 0.255 mA/cm^2 for Zn–Ni matrix to 0.1020 mA/cm^2 for Zn–Ni–Al_2O_3 composite coating containing 50 g /l nano-alumina.
- The data obtained from electrochemical impedance spectroscopy (EIS) assumes that, the charge transfer resistance (R_{ct}) is higher and the capacity of the double layer (C_{dl}) value

DOI 10.12776/ams.v22i3.706 p-ISSN 1335-1532
e-ISSN 1338-1156

is lower for Zn–Ni–Al2O3 composite coating containing 50 g /l nano-alumina alloy compared with those of Zn–Ni matrix. This behavior is in good agreement with that obtained from Tafel plot measurements.

- The study of nucleation has determined the growth electrochemical processes in the first moments following an instantaneous nucleation mode in three dimensions (3D) controlled diffusional

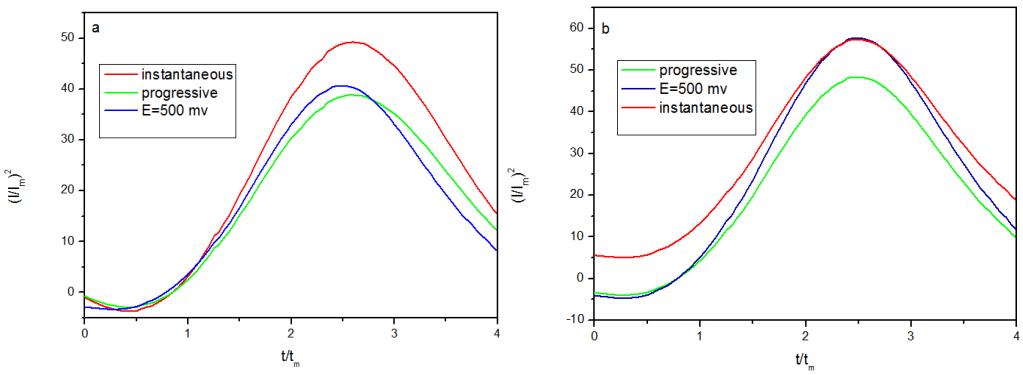

Fig. 7 Surface morphology of (a) Zn–Ni alloy coatings and (b) Zn–Ni–Al_2O_3 (30 g /l Al_2O_3) Composite coatings deposited at 30 mA/cm^2, T = 30 °C, and pH 3-4,5 for 60 s.

References

[1] A. Conde, M. A. Arenas, J. J. de Damborenea: Corrosion Science, Vol. 53 , No. 4, 2011, p. 1489–1497, doi:10.1016/j.corsci.2011.01.021

[2] S. Ghaziof, W. Gao: Applied Surface Science, Vol. 311, 2014, p. 635–642, doi:10.1016/j.apsusc.2014.05.127

[3] T.V. Byk , T.V. Gaevskaya, L.S. Tsybulskaya: Surface & Coatings Technology, Vol. 202, No. 24, 2008, p. 5817–5823, doi:10.1016/j.surfcoat.2008.05.058

[4] O. Hammami, L. Dhouibi, P. Berçot, M. Rezrazi, E. Triki: Surface & Coatings Technology, Vol. 203, 2009, No. 19, p. 2863–2870, doi: 10.1016/j.surfcoat.2009.02.129

[5] R. Ramanauskas, R. Juskenas, A. Kalinicenko, L. F. G. Mesias: Journal of Solid State Electrochemistry, Vol. 8, 2004, No. 6, p 416–421, doi:10.1007/s10008-003-0444-2

[6] N. Eliaz, K. Venkatakrishna, A. Chitharanjan Hegde: Surface & Coatings Technology, Vol. 205, No. 7, 2010, p.1969–1978, doi:10.1016/j.surfcoat.2010.08.077

[7] A. C. Hegde, K. Venkatakrishna, N. Elia: Surface & Coatings Technology, Vol. 205, 2010, No.7, p. 2031–2041, doi:10.1016/j.surfcoat.2010.08.102

[8] M. Diafi, N. Belhamra, H. Ben Temam, B.Gasmi, S. Benramache: Acta Metallurgica Slovaca, Vol. 21, No. 3, 2015, p. 226-235, doi: 10.12776/ams.v21i3.472

[9] S. Ghaziof, W. Gao: Journal of Alloys and Compounds, Vol. 622, 2015, p. 918–924 doi:.org/10.1016/j.jallcom.2014.11.025

[10] S. Ghaziof, P. A. Kilmartin, W.Gao: Journal of Electroanalytical Chemistry, Vol .755 , 2015, p. 63–70, doi: org/10.1016/j.jelechem.2015.07.041

[11] O. Hammami, L. Dhouibi, P. Berçot, E. Rezrazi: Journal of Applied Electrochemistry, Vol. 44, No. 1, 2014, p.115–121, doi: 10.1007/s10800-013-0613-7

[12] L. Shi, C. Sun, P. Gao, F. Zhou, L. Weimin: Applied Surface Science, Vol.252, No. 10, 2006, p.3591–3599, doi:10.1016/j.apsusc.2005.05.035

[13] O. Hammami, L. Dhouibi, P. Berçot, E. Rezrazi, E. Triki : Hindawi Publishing Corporation International Journal of Corrosion, Vol. 2012, Article ID 301392, 8 pages, doi:10.1155/2012/301392
[14] S. Pouladi , M. H. Shariat, M. E. Bahrololoom: Surface & Coatings Technology, Vol. 213, 2012, p. 33–40, doi.org/10.1016/j.surfcoat.2012.10.011
[15] H. Yu Zheng, M. Zhong An: Journal of Alloys and Compounds, Vol. 459, No.1-2 ,2008, p. 548–552, doi.10.1016/j.jallcom.2007.05.043
[16] P. C. Tulio, S. E.B. Rodrigues, I. A. Carlos :Surface & Coatings Technology, Vol. 202 , No. 1, 2007 , p. 91–99, doi:10.1016/j.surfcoat.2007.04.084
[17] A. Gome, I. Almeida , T. Frade, A. C. Tavares: Journal of Nanoparticle Research ,2012 , 13pages ,doi: 10.1007/s11051-011-0692-5
[18] C. Müller, M. Sarret, M. Benballa: Surface and Coatings Technology,Vol. 162, No. 1, 2003, p. 49–53, doi:10.1016/S0257-8972(02)00360-2
[19] K. R. Sriraman, S. Brahimi, J. A. Szpunar, J. H. Osborned, S. Yue: Electrochimica Acta,Vol. 105, 2013, p. 314– 323, doi:10.1016/j.electacta.2013.05.010
[20] M. Diafi, M. Omari: Boletín de la Sociedad Española de Cerámica y Vidrio, Vol. 51, No. 6, 2012, p. 337-342, doi: 10.3989/cyv.462012
[21] R . Sekar , K . K . Jagadesh, G. N. K. Ramesh bapu: , Transcations of Nonferrous Metals Society of China, Vol.25, N.6 ,2015, p.1961−1967, DOI: 10.1016/S1003-6326(15)63804-3
[22] S. H. Mosavat, M. H. Shariat, M. E. Bahrololoom: Corrosion Science, Vol. 59, 2012, p. 81–87, doi:10.1016/j.corsci.2012.02.012
[23] W. Chen, W. Gao: Electrochimica Acta, Vol. 55, 2010, No. 22, p. 6865–6871, Doi:10.1016/j.electacta.2010.05.079.
[24] K. R. Sriraman, H. W. Strauss, S. Brahimi, R. R. Chromik, J. A. Szpunar, J. H. Osborne: Tribology International, Vol. 56, 2012, p. 107–120, doi:10.1016/j.triboint.2012.06.008
[25] A. M. Alfantazi, U. Erb: Materials Science and Engineering A, vol .212, 1996, No. 1 , p.123–129, doi:10.1016/0921-5093(96)10187-8
[26] B. Subramanian, S. Mohan, Sobha Jayakrishnan: Surface & Coatings Technology ,Vol. 201, No.3-4, ,2006,p. 1145–1151, Doi:10.1016/j.surfcoat.2006.01.042
[27] A. R. El-Sayed, H. S. Mohran, H. M. Abd El-Lateef: Journal of Power Sources, Vol. 195 , No. 19, 2010, p .6924–6936, doi: 10.1016/j.jpowsour.2010.03.071
[28] H. M. Abd El-Lateef, A. R. El-Sayed, H. S. Mohran: Transcations of Nonferrous Metals Society of China, Vol. 25, No. 8, 2015, p. 2807−2816, doi: 10.1016/S1003-6326(15)63906-1
[29] B. Scharifker, G. Hills: Electrochim Acta, Vol. 28, No. 7, 1983, p. 879–889, doi:10.1016/0013-4686(83)85163-9
[30] N. Eliaz, M. Eliyahu: Journal of Biomedical Materials Research Part A, 2006, p. 621–634, doi: 10.1002/jbm.a.30944
[31] K. Raeissi, A. Saatchi, M. A. Golozar: Journal of Applied Electrochemistry, Vol. 33, 2003, No. 7, p. 635–642, doi: 10.1023/A:1024914503902

Acknowledgments
I would like to thanks "Responsible of LABORATORY OF THIN FILMS AND APPLICATIONS" FOR THEIR ASSISTANCE IN THE PREPARATION OF THIS WORK.